PCCP

Volume 1 | Number 1 | Jan 2013 | Pages 1–100

PCCP

Physical Chemistry Chemical Physics
www.rsc.org/pccp

ROYAL SOCIETY OF CHEMISTRY

ROYAL SOCIETY OF CHEMISTRY

www.rsc.org/pccp

ARTICLE TYPE

Quantum Entanglement in Carbon-Carbon, Carbon-Phosphorus and Silicon-Silicon Bonds[†]

Matthieu Mottet[a], **Paweł Tecmer,**[*a‡] **Katharina Boguslawski,**[*a‡] **Örs Legeza,**[b] **and Markus Reiher**[a]

The chemical bond is an important local concept to understand chemical compounds and processes. Unfortunately, like most local concepts, the chemical bond and the bond order do not correspond to any physical observable and thus cannot be determined as an expectation value of a quantum chemical operator. We recently demonstrated [Boguslawski *et al., J. Chem. Theory Comput.*, 2013, **9**, 2959–2973] that one- and two-orbital-based entanglement measures can be applied to interpret electronic wave functions in terms of orbital correlation. Orbital entanglement emerged to be a powerful tool to provide a qualitative understanding of bond-forming and bond-breaking processes, and allowed for an estimation of bond orders of simple diatomic molecules beyond the classical bonding models. In this article we demonstrate that the orbital entanglement analysis can be extended to polyatomic molecules to understand chemical bonding.

1 Introduction

Albeit computational chemistry has reached a remarkable level in the quantitative description of atoms and molecules [1–4], these achievements came along with a fading qualitative understanding. To remedy the receding interpretation of complex total electronic wave functions, quantum chemistry introduced various analysis tools based on local properties, that is properties of atoms or functional groups of atoms in a molecule, like, for instance, bond orders, atomic charges in molecules and local spins [5–22]. Such local concepts allow us to interpret electronic structures in terms of intuitive building blocks and favor a qualitative understanding of chemical processes. Similar approaches such as hardness, softness, electronegativity and related properties emerged within conceptual density functional theory [23].

The bond order [24–32] is an important and popular local concept to understand chemical bonding. It constitutes a quantitative measure for the formal number of (covalent and ionic) bonds formed between two neighboring atoms. The bond order can elucidate the stability and the strength of a chemical bond and can be thus considered as a guide to chemical synthesis. Unfortunately, the chemical bond or the bond order cannot be unambiguously assigned to any quantum chemi-

cal observable. As a consequence, various bond order concepts have been introduced in quantum chemistry for both one-determinant [27,28,33,34] and correlated wave functions [35,36].

Conceptually different bond-order measures have been developed for one-determinant wave functions that are based on a simple electron counting scheme [37–40] and thus provide an intuitive and convenient picture of the chemical bond. An extension of the electron-counting scheme to correlated wave functions was presented by Roos *et al.* [40] who introduced an effective bond order between two atomic centers that is based on natural occupation numbers of molecular orbitals and thus determined from a one-particle density matrix. As the natural occupation numbers may have non-integer values, the resulting effective bond orders will be non-integer, as well. The true bond order is defined as the lowest integer larger or equal to the total effective bond order value.

Alternatively, the nature of the chemical bond can be investigated using concepts from quantum information theory [41–47]. Following the observation that one- and two-orbital-based entanglement measures provide quantitative means for an assessment and classification of electron correlation effects among molecular orbitals [46,48], an entanglement analysis on bond-formation and dissociation processes of diatomic molecules [47] was presented by some of us. Our entanglement study indicated that concepts from quantum information theory can be used to retrieve deeper insights into electronic structures and molecular processes. Furthermore, entanglement measures based on many-particle reduced density matrices offer a conceptual understanding of bond-forming and bond-breaking processes. The entanglement analysis comprises two entropic measures which quantifies the quantum information

exchange between molecular orbitals and molecular orbital pairs[45,47]; (i) The single-orbital entropy that is determined from the eigenvalues $w_{\alpha,i}$ of the one-orbital reduced density matrix of a given orbital i,

$$s(1)_i = -\sum_{\alpha=1}^{4} w_{\alpha,i} \ln w_{\alpha,i}, \qquad (1)$$

where α runs over all local states of one molecular orbital (there are 4 in the case of spatial orbitals). (ii) The mutual information that measures the correlation of two orbitals embedded in the environment of all other active space orbitals,

$$I_{i,j} = \frac{1}{2}[s(1)_i + s(1)_j - s(2)_{i,j}](1 - \delta_{ij}) \qquad (2)$$

where $i, j = 1 \ldots k$ is the orbital index of all k active space orbitals and δ_{ij} the Kronecker delta[49]. In the above equation, $s(2)_{i,j}$ is the two-orbital entropy and is determined from the eigenvalues $w_{\alpha,i,j}$ of the two-orbital reduced density matrix $\rho_{i,j}$ of orbital pair $\{i, j\}$ [47],

$$s(2)_{i,j} = -\sum_{\alpha=1}^{16} w_{\alpha,i,j} \ln w_{\alpha,i,j}. \qquad (3)$$

So far, the entanglement analysis has been applied to the dissociation process of simple diatomic molecules, while its application to larger molecular systems has not been investigated, yet. In this work, we will study the performance of orbital-based entanglement measures in resolving bond-breaking processes and in dissecting electronic structures in terms of entangled molecular orbital building blocks for a number of diatomic and polyatomic molecules. Our set of prototypical molecules covers singly, doubly and triply bonded carbon–carbon, carbon–phosphorus and silicon–silicon centers.

2 Methodology

2.1 Structure optimization

All molecular structures were optimized using the Amsterdam Density Functional program package[50–52] employing the BP86[53,54] exchange–correlation functional and the Triple-ζ Polarization basis set[55]. The bond lengths of the two dissociating centers (cf. Table 1 for equilibrium bond lengths) were systematically varied while the structure of the fragments connected to these centers was relaxed (constrained geometry optimization). The optimized structures of all polyatomic molecules can be found in Tables I–VI of the Supporting Information.

Table 1 Summary of equilibrium bond lengths, r_e, Abelian point group symmetries and active space sizes used for CASSCF and DMRG calculations for all molecules. In the standard (x, y) notation for active spaces, where x indicates the number of correlated electrons and y number of correlated orbitals.

Molecule	$r_e[\text{Å}]$	Symmetry	CASSCF	DMRG
C_2	$r_{C-C} = 1.34$	D_{2h}	$(8, 8)$	$(8, 26)$
$[CP]^-$	$r_{C-P} = 1.62$	C_{2v}	$(10, 8)$	$(10, 26)$
HCP	$r_{C-P} = 1.55$	C_{2v}	$(10, 9)$	$(10, 26)$
C_2H_2	$r_{C-C} = 1.21$	D_{2h}	$(10, 10)$	$(10, 28)$
C_2H_4	$r_{C-C} = 1.34$	D_{2h}	$(12, 12)$	$(12, 28)$
C_2H_6	$r_{C-C} = 1.53$	C_{2h}	$(14, 14)$	$(14, 28)$
Si_2H_2	$r_{Si-Si} = 2.11$	C_{2h}	$(10, 10)$	$(10, 26)$
Si_2H_4	$r_{Si-Si} = 2.15$	D_{2h}	$(12, 12)$	$(12, 28)$

2.2 CASSCF

All Complete Active Space Self-Consistent Field[56–58] (CASSCF) calculations have been performed using the MOL-PRO 2010.1 program package[59]. As active space, the full valence shell was taken for all molecular systems (*i.e.* H: $1s$; C: $2s$, $2p_x$, $2p_y$ and $2p_z$; Si, P: $3s$, $3p_x$, $3p_y$ and $3p_z$). For the C_2, C_2H_2, C_2H_4 and Si_2H_4 molecules, D_{2h} point group symmetry was imposed, while for HCP and $[CP]^-$ C_{2v} point group symmetry was used. For C_2H_6 and Si_2H_2, C_{2h} point group symmetry was set. All CASSCF active space sizes are summarized in Table 1.

For all molecules but C_2, Dunning's cc-pVTZ basis set was used with the following contractions H: $(5s, 2p, 1d) \rightarrow [3s, 2p, 1d]$; C, N: $(10s, 5p, 2d, 1f) \rightarrow [4s, 3p, 2d, 1f]$[60]; Si, P: $(15s, 9p, 2d, 1f) \rightarrow [5s, 4p, 2d, 1f]$[61]. In the case of C_2, the large aug-cc-pVTZ basis set (C: $(11s, 6p, 3d, 2f) \rightarrow [5s, 4p, 3d, 2f]$[60]) was chosen.

2.3 DMRG

All DMRG calculations were performed with the BUDAPEST DMRG program[62]. As orbital basis, the natural orbitals obtained from the CASSCF calculations as described in the previous section were used. The active spaces were extended by including additional virtual Fock-type orbitals for each molecule as summarized in Table 1; $4a_g$, $2b_{3u}$, $2b_{2u}$, $1b_{1g}$, $4b_{1u}$, $2b_{2g}$, $2b_{3g}$ and $1a_u$ for C_2 and C_2H_2, $3a_g$, $2b_{3u}$, $2b_{2u}$, $1b_{1g}$, $3b_{1u}$, $2b_{2g}$, $2b_{3g}$ and $1a_u$ for Si_2H_4, $3a_g$, $4b_{3u}$, $2b_{2u}$, $2b_{1g}$, $2b_{1u}$, $1b_{2g}$, $1b_{3g}$ and $1a_u$ for C_2H_4 , $8a_1$, $4b_1$, $4b_2$ and $2a_2$ for CP and HCP (one a_1 orbital less was added to HCP), $5a_g$, $3a_u$, $5b_u$ and $3b_g$ for Si_2H_2, and finally, $5a_g$, $2a_u$, $5b_u$ and $2b_g$ for C_2H_6. We refer the reader to Table 2 for the correspondence of irreducible representations of Abelian subgroups chosen in the calculations of linear molecules and the full point group symmetry ($D_{\infty h}$ and $C_{\infty v}$).

To enhance DMRG convergence, the orbital ordering was

optimized[45] and the number of renormalized active-system states was chosen dynamically according to a predefined threshold value for the quantum information loss[63] employing the dynamic block state selection approach[64,65]. As an initial guess, the dynamically extended active-space (DEAS) procedure was applied[63]. In the DMRG calculations, the minimum and maximum number of renormalized active-system states was set to 512 and 1024, respectively, while the quantum information loss χ was set to 10^{-5} in all calculations. For the C_2 molecule it was necessary to increase the maximal number of renormalized active system states to 2048. The notation DMRG$(x,y)[m_{max}, m_{min}, \chi]$ indicates that x electrons are correlated in y orbitals, while the minimal and maximal number of active-system states was set to m_{min} and m_{max}, respectively. The minimal number of active-system states during the DEAS initialization procedure was set equal to m_{max} in all calculations.

The convergence behavior of all DMRG calculations with respect to the DMRG parameter set is discussed in the Supporting Information.

All entanglement measures, *i.e.*, the single-orbital entropy (Eq. (1)) and the mutual information (Eq. (2)), have been determined from converged DMRG wave functions for all molecules investigated.

Table 2 Resolution of the relevant irreducible representations of $D_{\infty h}$ and $C_{\infty v}$ point groups in terms of those of the D_{2h}, C_{2v} and C_{2h} subgroups[66].

$D_{\infty h}$	D_{2h}	$C_{\infty v}$	C_{2v}	C_{2h}
σ_g	a_g	σ	a_1	a_g
σ_u	b_{1u}	σ	a_1	b_u
π_g	$b_{2g} \oplus b_{3g}$	π	$b_1 \oplus b_2$	$a_g \oplus b_g$
π_u	$b_{2u} \oplus b_{3u}$	π	$b_1 \oplus b_2$	$a_u \oplus b_u$
δ_g	$a_g \oplus b_{1g}$	δ	$a_1 \oplus a_2$	$a_g \oplus b_g$
δ_u	$a_u \oplus b_{1u}$	δ	$a_1 \oplus a_2$	$a_u \oplus b_u$
ϕ_g	$b_{2g} \oplus b_{3g}$	ϕ	$b_1 \oplus b_2$	$a_g \oplus b_g$
ϕ_u	$b_{2u} \oplus b_{3u}$	ϕ	$b_1 \oplus b_2$	$a_u \oplus b_u$

3 Interpretation of entanglement diagrams

To illustrate the entanglement measures of Eqs. (1) and (2), we use a diagrammatic representation of the mutual information and single-orbital entropies as discussed in Refs. 46,47. Specifically, in the mutual information diagram, all orbitals are arranged on a circle and sorted clockwise according to their CASSCF occupation numbers and irreducible representation, respectively. The virtual Fock-type orbitals are sorted with respect to their energy eigenvalue. Each line in the $I_{i,j}$ diagram corresponds to the order of magnitude of $I_{i,j}$ values between orbital pair $\{i, j\}$ (calculated from Eq. (2)), while the

magnitude of the mutual information $I_{i,j}$ between each orbital pair $\{i, j\}$ is color-coded; strongly entangled orbitals are connected via blue lines ($I_{i,j} \approx 10^{-1}$), moderately entangled orbitals are linked by red lines ($I_{i,j} \approx 10^{-2}$), while weakly entangled orbital pairs are indicated by green lines ($I_{i,j} \approx 10^{-3}$).

The single-orbital entropies, Eq. (1), and mutual information, Eq. (2), corresponding to molecular orbitals associated with a chemical bond, *i.e.*, the bonding and antibonding orbital pairs, are large ($s(1)_i > 0.4$ and $I_{i,j} \approx 10^{-1}$) when bonds are stretched, while the remaining (active space) orbitals are only moderately ($0.1 < s(1)_i < 0.4$ and $I_{i,j} \approx 10^{-2}$) or weakly entangled ($s(1)_i < 0.1$ and $I_{i,j} \approx 10^{-3}$)[47]. Thus, in the dissociation limit, each bonding and antibonding orbital pair that is important to describe chemical bonding between two centers becomes strongly entangled and renders the dominant contributions in the $I_{i,j}$ and $s(1)_i$ diagrams. This observation provides a qualitative picture of the bond multiplicity between two centers. An entanglement-based (or entropic) bond order can be determined from the total number of steep changes in the $s(1)_i$-diagram observed in the dissociation limit after dividing by two to account for the bonding and antibonding combinations of molecular orbitals.

The increase in quantum entanglement observed when bonded atomic or molecular fragments are pulled apart can be mapped onto the concept of electron correlation: if bonds are stretched, the molecular system is said to have a strong multireference character where strong (static and nondynamic) electron correlation effects become dominant. In particular, molecular orbitals that are important for a correct description of nondynamic electron correlation are strongly entangled (large single-orbital entropies and mutual information)[46,47].

Furthermore, the rate of growth in $s(1)_i$ depends on the type (or entanglement strength) of a specific bond as the one- and two-orbital entanglement measures are derived from the electronic wave function[47]. For instance, $s(1)_i$ of orbitals involved in weak π-bonds increase faster than those corresponding to strong σ-bonds. A chemical bond is considered to be broken when $s(1)_i$ reaches its maximum value of $\ln 4 \approx 1.386$. Hence, a quantum entanglement analysis allows us to qualitatively resolve bond-breaking processes of individual σ-, π-, etc., bonds in multi-bonded centers[47].

It is important to stress that our orbital-based entanglement measures ($I_{i,j}$ and $s(1)_i$) remain unaffected by the choice of the size of the active space under the condition that the active space is balanced and provides an appropriate description of strong electron correlation effects. For all systems investigated in this work, full-valence (CASSCF) or extended full-valence (DMRG) active spaces allow for a correct description of static and nondynamic electron correlation and results in similar entropic bond orders[47].
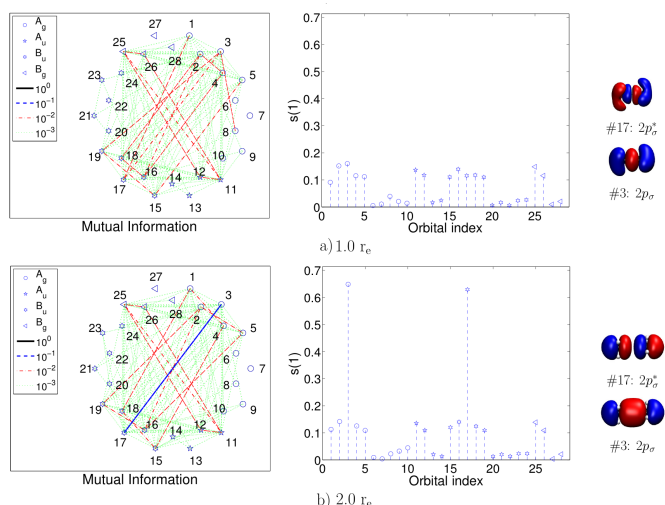
Fig. 1 Mutual information and single orbital entropies $s(1)_i$ for DMRG(14,28)[1024, 512, 10^{-5}] calculations for the C_2H_6 ($r_e = 1.53$) molecule at different inter-atomic distances. The orbitals are numbered and sorted according to their (CASSCF) natural occupation numbers. Strongly entangled orbitals are shown on the right-hand side. Each orbital index in the $s(1)_i$ diagram indicates one molecular orbital and corresponds to the same natural orbital as numbered in the mutual information plot (starting of index 1 and proceeding clockwise).

4   Results

4.1   Bonding between two carbon centers

4.1.1   Assessing the accuracy of entanglement-based bond orders for polyatomic molecules. The carbon–carbon bond is a fairly strong covalent bond, which gives rise to an enormous variety of organic molecules. The strength of this bond largely depends on its multiplicity; the higher the multiplicity the stronger the carbon–carbon bond. It is well-known and generally accepted that the carbon–carbon bond is weakest in alkanes, stronger in alkenes, and strongest in alkynes, where singly-, doubly- and triply- bonded centers are formed, respectively[67]. In this study, we choose the three lightest carbon-containing representatives of the hydrocarbon series ethane (C_2H_6), ethene (C_2H_4), and acetylene (C_2H_2). These molecules represent a prototypical test set to study the bond multiplicities in polyatomic molecules by means of quantum entanglement[47].

Figure 1 shows the mutual information and single-orbital entropies obtained from DMRG(14,28) calculations for the C_2H_6 molecule at two different carbon–carbon distances: $1.0r_e$ and $2.0r_e$ (additional entanglement diagrams for $0.8r_e$ and $1.5r_e$ can be found in the Supporting Information). At the inter-nuclear distance of $1.0r_e$, all orbitals are moderately
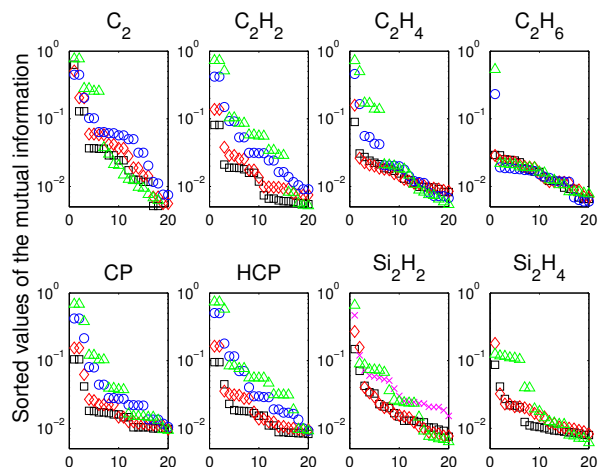

Fig. 2 Decay of the largest values of the mutual information ($I_{i,j} > 0.005$) for all molecules and inter-atomic distances investigated in this work. The symbols □, ◇, ○, × and △ stand for r=0.8, $1r_e$, $1.5r_e$, $1.65r_e$, $2r_e$, respectively.

and weakly entangled and it remains rather difficult to identify the bonding and antibonding combinations of molecular orbitals corresponding to the single-bond of interest. When the H_3C fragments are stretched from their equilibrium geometry, a gradual increase in mutual information and single-orbital entropies can be observed for the bonding and antibonding p_σ-orbitals (*cf.* Supporting Information for the $1.25r_e$ and $1.50r_e$ distances). The single-orbital entropy for the bonding-antibonding orbital pair (#3 and #17) reaches the value of about 0.7 in the vicinity of dissociation as shown in Figure 1. We should note that jumps in the mutual information can be indeed observed that occur around $I_{ij} \approx 10^{-1}$ (strongly entangled orbitals) and $I_{ij} \approx 10^{-2}$ (moderately entangled orbitals). Figure 2 shows the decay of the 20 largest contributions to I_{ij} for all investigated molecules and inter-atomic distances. Our entanglement analysis correctly predicts a bond order of 1 between the two carbon centers of C_2H_6 (cf. Figure 1).

The quantum entanglement study of the C_2H_4 molecule determined from DMRG(12,28) wave functions is illustrated in Figure 3 (and Figure 2 of the Supporting Information). We obtain a similar entanglement profile as for C_2H_6, though the bonding and antibonding p_π-orbitals are now more strongly entangled around the equilibrium structure than the bonding and antibonding p_σ-orbitals. Pulling the CH_2 fragments apart, weakens first the π-bond followed by the (stronger) σ-bond (see Figure 2 of the Supporting Information for a complete picture). The entanglement-based bond order of carbon–carbon in the C_2H_4 molecule is equal to 2.

The carbon–carbon bond in C_2H_2 is dissected in Figure 4.
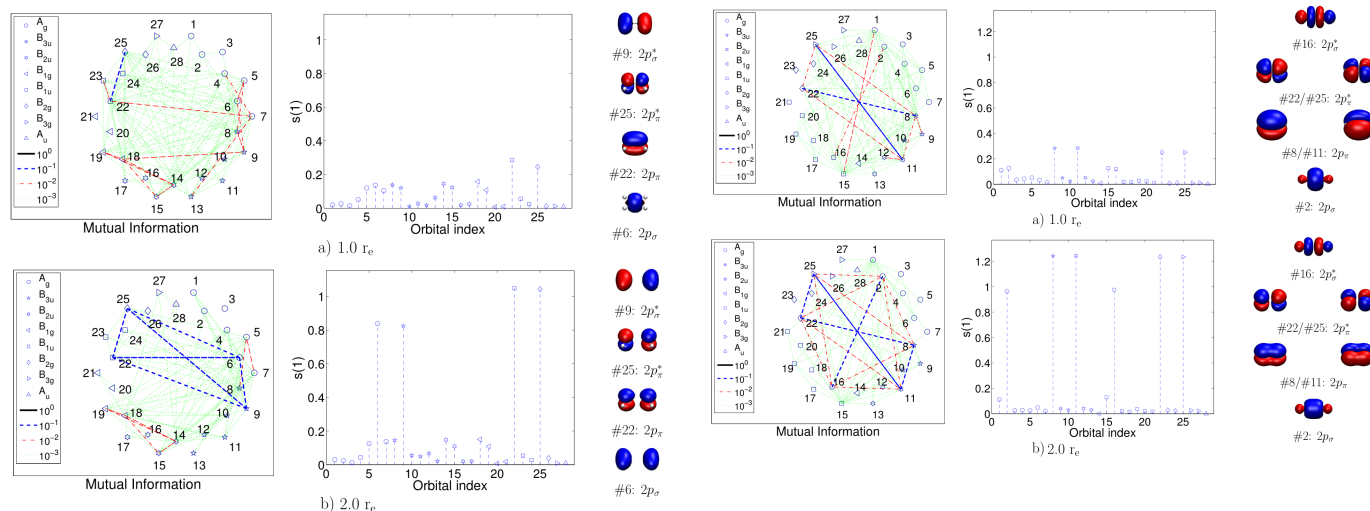
Fig. 3 Mutual information and single orbital entropies $s(1)_i$ for DMRG(12,28)[1024, 512, 10^{-5}] calculations for the C_2H_4 ($r_e = 1.34$) molecule at different inter-atomic distances. The orbitals are numbered and sorted according to their (CASSCF) natural occupation numbers. Strongly entangled orbitals are shown on the right-hand side. Each orbital index in the $s(1)_i$ diagram indicates one molecular orbital and corresponds to the same natural orbital as numbered in the mutual information plot (starting of index 1 and proceeding clockwise).

Fig. 4 Mutual information and single orbital entropies $s(1)_i$ for DMRG(10,28)[1024, 512, 10^{-5}] calculations for the C_2H_2 ($r_e = 1.21$) molecule at different inter-atomic distances. The orbitals are numbered and sorted according to their (CASSCF) natural occupation numbers. Strongly entangled orbitals are shown on the right-hand side. Each orbital index in the $s(1)_i$ diagram indicates one molecular orbital and corresponds to the same natural orbital as numbered in the mutual information plot (starting of index 1 and proceeding clockwise).

Similar to C_2H_4, four orbitals (#8, #11, #22 and #25) have slightly higher values for the single-orbital entropy than all remaining orbitals ($s(1)_i = 0.2$ vs. $s(1)_i = 0.1$) around the equilibrium distance. These are the doubly degenerate C $2p_\pi$- and C $2p_{\pi^*}$-orbitals. Stretching the CH fragments increases, as expected, first the orbital entanglement of the C $2p_\pi/2p_{\pi^*}$-orbitals, followed by the bonding and antibonding combination of the C $2p_z$ atomic orbitals. The entanglement diagram at 2.0r_e in the bottom panel of Figure 4 correctly predicts a triple bond between the two carbon centers in the C_2H_2 molecule.

In summary, our entanglement-based approach for determining bond orders, originally introduced for diatomic molecules, is transferable to polyatomic molecules and correctly predicts single, double and triple bond orders between the carbon–carbon centers in ethane, ethene and acetylene, respectively.

4.1.2 Notorious case of bonding in C_2. The formal bond order of C_2 remains a challenge for present-day chemistry. While multireference configuration interaction calculations on the carbon dimer suggested a bond order of 2 (cf. Ref. 68), a bond order of 4 has been anticipated, as well[69–72]. However, the presence of a quadruple bond in C_2 has been discarded in the most recent Generalized Valence-Bond (GVB) study presented in Ref. 73. Taking into account the fact that an accu-

rate quantum chemical description of the C_2 molecule requires a multireference method[32,68,73–81], a DMRG study combined with a quantum entanglement analysis can provide a complementary entropic perspective on the nature of bonding in C_2.

As summarized in Figure 5, the C_2 molecule contains strongly entangled orbitals (#2 and #14) already around the equilibrium distance (compare Figure 5 and Figures 1, 3 and 4). These strongly correlated orbitals correspond to the $2p_\sigma$ and $2p_{\sigma^*}$ molecular orbitals. When the two carbon atoms are pulled apart, the single-orbital entropies associated with the $2p_\sigma/2p_{\sigma^*}$-orbital pair (#2 and #14) gradually decrease from 0.8 at 0.8r_e to less than 0.2 at 2.0r_e. Simultaneously, the entanglement of the degenerate $2p_\pi$ and $2p_{\pi^*}$ molecular orbital pairs increases from 0.3 at 0.8r_e to 1.2 at 2.0r_e.

We should note that, based on our observations, a true π-bond is associated with strongly entangled p_π/p_{π^*}-orbital pairs, which comprises larger $s(1)_i$-values than those obtained for σ/σ^*-orbital pairs. A separation of the carbon–carbon centers to 2.0r_e gives rise to the traditional π-double bond (dominant contributions to $s(1)_i$) similar to that found in acetylene, while the $2p_\sigma/2p_{\sigma^*}$-orbital pairs do not participate in the chemical bonding (vanishing $s(1)_i$). Around the bond-breaking region of 1.5r_e, we observe a gradual transition of the singly-bonded C_2 molecule, over two triply-bonded centers to a purely doubly-bonded system.
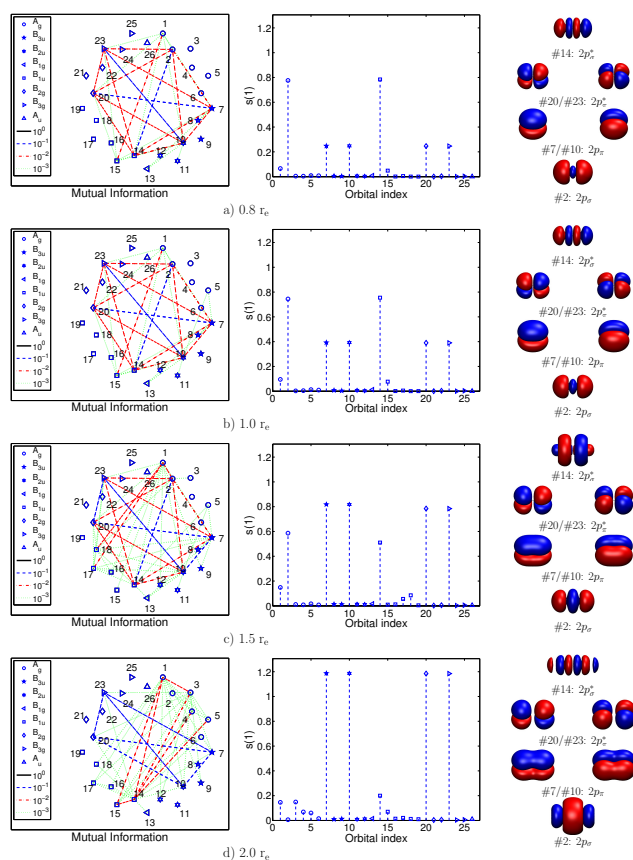
Fig. 5 Mutual information and single orbital entropies $s(1)_i$ for DMRG(8,26)[2048, 512, 10^{-5}] calculations for the C_2 ($r_e = 1.24$) molecule at different inter-atomic distances. The orbitals are numbered and sorted according to their (CASSCF) natural occupation numbers. Strongly entangled orbitals are shown on the right-hand side. Each orbital index in the $s(1)_i$ diagram indicates one molecular orbital and corresponds to the same natural orbital as numbered in the mutual information plot (starting of index 1 and proceeding clockwise).

Our observations underline the complex nature of the chemical bond in the C_2 molecule, which clearly deviates from the classical bonding prototype of single, double and triple bond. Finally, it is important to note that our entanglement analysis is in agreement with the most recent GVB study[73]; elucidating that the C_2 molecule around the equilibrium distance is well-described "as having a traditional covalent σ-bond". However, our entanglement analysis cannot resolve the antiferrmagnetically coupled electrons in the remaining π-orbitals[32,73], due to delocalized natural orbital basis used in this study, where all states equally contribute to $s(1)_i$ (see Figure VII of the Supporting Information, where the contribution of each component of the single-orbital entropy is presented).
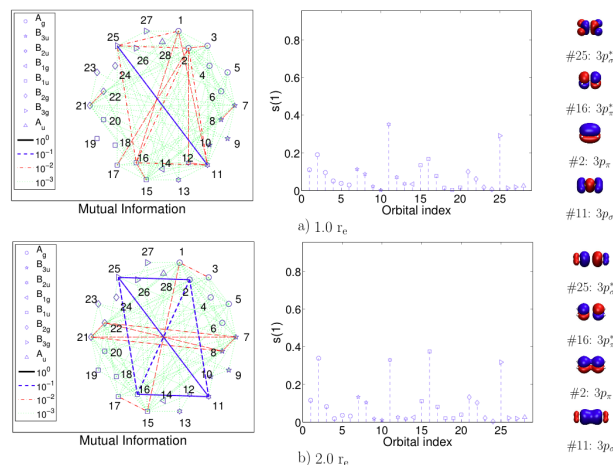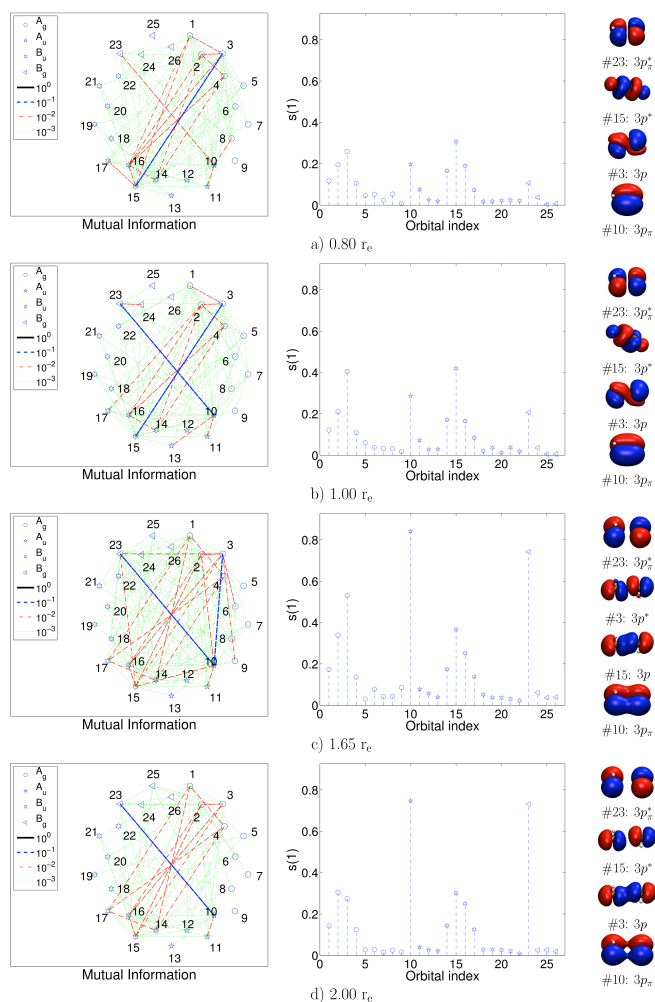

Fig. 6 Mutual information and single orbital entropies $s(1)_i$ for DMRG(12,28)[1024, 512, 10^{-5}] calculations for the Si_2H_4 ($r_e = 2.15$) molecule at different inter-atomic distances. The orbitals are numbered and sorted according to their (CASSCF) natural occupation numbers. Strongly entangled orbitals are shown on the right-hand side. Each orbital index in the $s(1)_i$ diagram indicates one molecular orbital and corresponds to the same natural orbital as numbered in the mutual information plot (starting of index 1 and proceeding clockwise).

5   Entanglement in silicon-silicon bonding

Si_2H_2 and Si_2H_4 are heavier homologues of ethene and acetylene. They exhibit a peculiar nature of the chemical bond that is notably different from those between the carbon centers in C_2H_2 and C_2H_4, respectively[82]. The complexity of the chemical bond in these systems originates (a) from their "trans-bent" geometries[83–85] (by contrast, C_2H_4 is planar and C_2H_2 is linear in their equilibrium structures), (b) from the energetical preference for low-spin states located at the Si centers upon Si–Si bond dissociation[86–89], and (c) differences in the spatial distribution of s- and p-orbitals[5].

For simplicity, we imposed a planar geometry on the Si_2H_4 molecule. Figure 6 illustrates the performance of the entanglement-based bond analysis for Si_2H_4 obtained from DMRG(12,28) calculations. The entanglement diagrams are similar to those of C_2H_4 indicating doubly-bonded Si–Si centers. The double bond in the Si_2H_4 compound in its planar structure was also approved in recent theoretical studies[90–94].

Figure 7 depicts the entanglement profiles for breaking the Si–Si centers in the Si_2H_2 molecule, obtained form DMRG(10,28) calculations, where we imposed the "trans-bent" geometry close to the equilibrium. At $0.8r_e$ and $1.0r_e$, four orbitals are moderately entangled (#3, #10, #15, #23) that correspond to the $3p_n$- and $3p_{n*}$-orbitals (#3 and #10, lone-

Fig. 7 Mutual information and single orbital entropies $s(1)_i$ for DMRG(10,26)[1024, 512, 10^{-5}] calculations for the Si_2H_2 ($r_e = 2.11$) molecule at different inter-atomic distances. The orbitals are numbered and sorted according to their (CASSCF) natural occupation numbers. Strongly entangled orbitals are shown on the right-hand side. Each orbital index in the $s(1)_i$ diagram indicates one molecular orbital and corresponds to the same natural orbital as numbered in the mutual information plot (starting of index 1 and proceeding clockwise).

pair type bonds[87]) and to the $3p_\pi$- and $3p_{\pi*}$-orbitals (#16 and #23), respectively. Stretching the Si–Si centers leads to structural changes from "trans-bent" to "trans-perpendicular" geometries (see Table VI of the Supporting Information for more details). Upon dissociation, the single-orbital entropy of orbitals involved in π-type bonding increases fastest and reaches a maximum value of 0.85 at $1.5r_e$. At larger inter-atomic Si–Si distances, $s(1)_i$ slightly decreases to 0.8, while the single-orbital entropies of the lone-pair orbital pairs de-

cline to about 0.3 around $2.0r_e$. This peculiar behavior is caused by structural changes and the reorientation of the Si–H fragments with respect to each other upon dissociation. The quantum-entanglement diagrams extracted at $2.0r_e$ point to a single π-type bonding in the Si_2H_2 molecule, supported by one weakly entangled bond attributed to the interaction between both Si lone-pairs. We should note, however, that this lone-pair 'bond'[87] comprises the most strongly entangled orbitals around the equilibrium structure.

The entanglement-based bond analysis agrees well with other theoretical findings that the Si_2H_2 molecule has a double bond in its "trans-bent" geometry and a single bond in its "trans-perpendicular" structure[87,89,95]. Our study also supports that the Si–Si bond in Si_2H_2 is a combination of one π- and one "donor–acceptor" lone-pair-bond[87,89].

6 Bond multiplicity in carbon–phosphorus centers

The discovery of phosphoalkynes by Gier[96] in 1961 paved the way the way for a new type of chemistry. The more diffuse nature of the phosphorus valence orbitals gives rise to a variety of interesting bonding properties with lighter first-row elements. Notably, the ground state of the phosphorus atom is a quadruplet, allowing for a formal triple bond with the carbon atom.
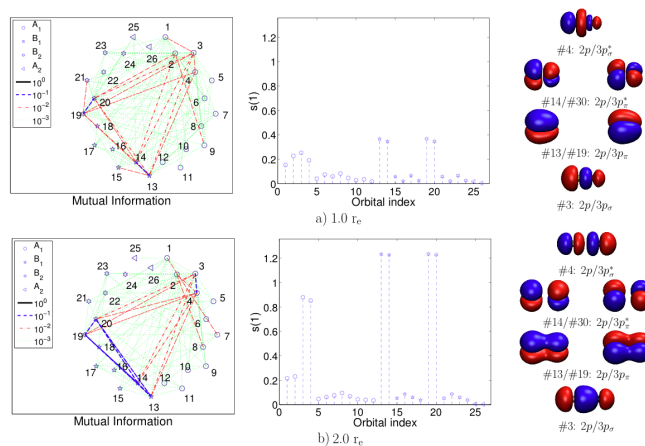
Fig. 8 Mutual information and single orbital entropies $s(1)_i$ for DMRG(10,26)[1024, 512, 10^{-5}] calculations for the $[CP]^-$ ($r_e = 1.62$) molecule at different inter-atomic distances. The orbitals are numbered and sorted according to their (CASSCF) natural occupation numbers. Strongly entangled orbitals are shown on the right-hand side. Each orbital index in the $s(1)_i$ diagram indicates one molecular orbital and corresponds to the same natural orbital as numbered in the mutual information plot (starting of index 1 and proceeding clockwise).

This hypothesis can be elucidated by studying the quantum entanglement of carbon–phosphorus bonding in the CP and [HCP$^-$] prototypical molecules. An entanglement-bond analysis based on DMRG(10,26) calculations is presented in Figures 8 and 9 for the CP and [HCP$^-$] moieties, respectively. At a distance of $1.0r_e$ in both molecules, the π/π^*-orbitals (#14, #13, #19, and #30) are moderately entangled while all other orbitals are only weakly entangled. Upon dissociation the single-orbital entropies associated with the degenerate π/π^*-orbital pairs, corresponding to the bonding and antibonding combinations of C $2p_\pi$- and P $3p_\pi$-orbitals, increase faster than those of the σ/σ^*-orbital pairs, (#3 and #4) which correspond to the bonding and antibonding combinations of C $2p_\sigma$- and P $3p_\sigma$-orbitals. In both molecules, the maximum of $s(1)_i$ for π-orbitals is reached at $2.0r_e$ and equals approximately 1.3. Additional presence of highly entangled σ-orbitals at this distance clearly indicates a triple bond between carbon and phosphorus in the CP and [HCP$^-$] molecules. The entanglement nature of this bond is quite similar to what we observed for the triply bonded carbon–carbon centers in the C_2H_2 molecule (cf. Figure 4) as well as to the triply bonded dinitrogen molecule discussed in Ref. 47. We should emphasize that all triply bonded centers studied possess similar decays of the mutual information as illustrated in Figure 2. Finally, it is worth to mention that our findings are in line with previously reported density functional theory studies of carbon–phosphorus bond-

ing in the [CP]$^-$ and HCP molecules[97].

7 Conclusions

We presented an entanglement-based bond order analysis of carbon–carbon, silicon–silicon and carbon–phosphorus centers. Our approach embraces the mutual information and single-orbital entropy and correctly reproduces bond multiplicities in simple polyatomic molecules like ethane, ethene and acetylene, and confirms the triple bonding between the carbon–phosphorus centers in the [CP]$^-$ and HCP molecules. The behavior of phosphorus in these prototypical phospho-alkynes closely resembles the bonding situation in the N_2 and C_2H_2 molecules.
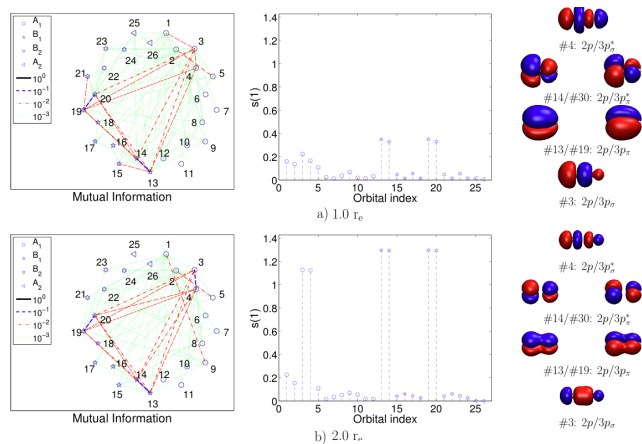
Furthermore, our analysis confirms that the nature of the chemical bond in the C_2 molecule is far more complicated than for their higher substituted analogs like C_2H_6, C_2H_4, and C_2H_2. Stretching the C–C bond in C_2 does not yield a gradually increasing entanglement pattern, which is an indication of the complexity of chemical bonding in the carbon dimer. We also observed such an exceptional behavior of chemical bonding between the Si–Si centers in the Si_2H_2 molecule which can be explained by structural rearrangements of the SiH fragments upon dissociation.

8 Acknowledgments

Fig. 9 Mutual information and single orbital entropies $s(1)_i$ for DMRG(14,28)$[1024,512,10^{-5}]$ calculations for the HCP ($r_e = 1.55$) molecule at different inter-atomic distances. The orbitals are numbered and sorted according to their (CASSCF) natural occupation numbers. Strongly entangled orbitals are shown on the right-hand side. Each orbital index in the $s(1)_i$ diagram indicates one molecular orbital and corresponds to the same natural orbital as numbered in the mutual information plot (starting of index 1 and proceeding clockwise).

References

1 R. Bartlett, *Comparison of Ab Initio Quantum Chemistry with Experiment for Small Molecules*, Springer, 1984.

2 T. Helgaker, P. Jørgensen and J. Olsen, *Molecular Electronic-Structure Theory*, Wiley, 2000.

3 R. J. Bartlett and M. Musiał, *Rev. Mod. Phys.*, 2007, **79**, 291–350.

4 A. J. Cohen, P. Mori-Sánchez and W. Yang, *Chem. Rev.*, 2012, **112**, 289.

5 W. Kutzelnigg, *Angew. Chem. Int. Ed. Engl.*, 1984, **23**, 272–295.

6 A. E. Clark and E. R. Davidson, *J. Chem. Phys.*, 2001, **115**, 7382–7392.

7 E. R. Davidson and A. E. Clark, *Mol. Phys.*, 2001, **100**, 373–383.

8 A. E. Clark and E. R. Davidson, *J. Phys. Chem. A*, 2002, **106**, 6890–6896.

9 C. Herrmann, M. Reiher and B. A. Hess, *J. Chem. Phys.*, 2005, **122**, 34102.

10 C. Herrmann, L. Yu and M. Reiher, *J. Comput. Chem.*, 2006, **27**, 1223–1239.

11 I. Mayer, *Chem. Phys. Lett.*, 2007, **440**, 357–359.

12 E. R. Davidson and A. E. Clark, *Phys. Chem. Chem. Phys.*, 2007, **9**, 1881–1894.

13 M. Reiher, *Faraday Discuss.*, 2007, **135**, 97–124.

14 M. Podewitz, C. Herrmann, A. Malassa, M. Westerhausen and M. Reiher, *Chem. Phys. Lett.*, 2008, **451**, 301–308.

15 D. R. Alcoba, L. Lain, A. Torre and R. C. Bochicchio, *Chem. Phys. Lett.*, 2009, **470**, 136–139.

16 I. Mayer, *Chem. Phys. Lett.*, 2009, **478**, 323–326.

17 M. Podewitz and M. Reiher, *Adv. Inorg. Chem.*, 2010, **62**, 177–230.

18 A. Torre, D. R. Alcoba, L. Lain and R. C. Bochicchio, *J. Phys. Chem. A*, 2010, **114**, 2344–2349.

19 I. Mayer and E. Matito, *Phys. Chem. Chem. Phys.*, 2010, **12**, 11308–11314.

20 D. R. Alcoba, A. Torre, L. Lain and R. C. Bochicchio, *J. Chem. Theory Comput.*, 2011, **7**, 3560–3566.

21 D. R. Alcoba, A. Torre, L. Lain and R. C. Bochicchio, *Chem. Phys. Lett.*, 2011, **504**, 236–240.

22 E. Ramos-Cordoba, E. Matito, I. Mayer and P. Salvador, *J. Chem. Theory Comput.*, 2012, **8**, 1270–1279.

23 P. Geerlings, F. De Proft and W. Langenaeker, *Chem. Rev.*, 2003, **103**, 1793–1873.

24 K. B. Wiberg, *Tetrahedron*, 1968, **24**, 1083–1096.

25 D. R. Armstrong, P. G. Perkins and J. J. P. Stewart, *J. Chem. Soc., Dalton Trans.*, 1973, 838–840.

26 M. A. Natiello and J. A. Medrano, *Chem. Phys. Lett.*, 1984, **105**, 180–182.

27 I. Mayer, *Theor. Chim. Acta*, 1985, **67**, 315–322.

28 I. Mayer, *Int. J. Quantum Chem.*, 1986, **29**, 73–84.

29 R. C. Bochicchio, *J. Mol. Struct.*, 1991, **228**, 209–225.

30 D. R. Alcoba, R. C. Bochicchio, L. Lain and A. Torre, *Chem. Phys. Lett.*, 2007, **442**, 157–163.

31 I. Mayer, *J. Comput. Chem.*, 2007, **28**, 204–221.

32 E. Ramos-Cordoba, P. Salvador and M. Reiher, *Chem. Eur. J.*, 2013, **19**, 15267–15275.

33 I. Mayer, *Chem. Phys. Lett.*, 1983, **97**, 270–274.

34 I. Mayer, *Int. J. Quantum Chem.*, 1986, **XXIX**, 477–483.

35 D. R. Alcoba, R. C. Bochicchio, L. Lain and A. Torre,

Phys. Chem. Chem. Phys., 2008, **10**, 5144–5146.

36 R. M. Lobayan, D. R. Alcoba, R. C. Bochicchio, A. Torre and L. Lain, *J. Phys. Chem. A*, 2010, **114**, 1200–1206.

37 G. Herzberg, *Z. Phys.*, 1929, **57**, 601–630.

38 M. B. Hall, *Polyhedron*, 1987, **6**, 679–684.

39 M. Brynda, L. Gagliardi, P.-O. Widmark, P. P. Power and B. O. Roos, *Angew. Chem. Int. Ed.*, 2006, **45**, 3804–3807.

40 B. O. Roos, A. C. Borin and L. Gagliardi, *Angew. Chem. Int. Ed.*, 2007, **46**, 1469–1472.

41 R. F. Nalewajski, *J. Phys. Chem. A*, 2000, **104**, 11940–11951.

42 R. F. Nalewajski, *Mol. Phys.*, 2004, **102**, 531–546.

43 R. F. Nalewajski, *J. Math. Chem.*, 2009, **47**, 692–708.

44 R. F. Nalewajski and P. Gurdek, *Struct. Chem.*, 2012, 1383–1398.

45 G. Barcza, O. Legeza, K. H. Marti and M. Reiher, *Phys. Rev. A*, 2011, **83**, 12508.

46 K. Boguslawski, P. Tecmer, O. Legeza and M. Reiher, *J. Phys. Chem. Lett.*, 2012, **3**, 3129–3135.

47 K. Boguslawski, P. Tecmer, G. Barcza, Ö. Legeza and M. Reiher, *J. Chem. Theory Comput.*, 2013, **9**, 2959–2973.

48 P. Tecmer, K. Boguslawski, O. Legeza and M. Reiher, *Phys. Chem. Chem. Phys*, 2014, **16**, 719–727.

49 J. Rissler, R. M. Noack and S. R. White, *Chem. Phys.*, 2006, **323**, 519–531.

50 ADF2012.01, SCM, Theoretical Chemistry, Vrije Universiteit, Amsterdam, The Netherlands, http://www.scm.com.

51 G. te Velde, F. M. Bickelhaupt, S. J. A. van Gisbergen, C. F. Guerra, E. J. Baerends, J. G. Snijders and T. Ziegler, *J. Comput. Chem.*, 2001, **22**, 931–967.

52 C. F. Guerra, J. G. Snijders, G. te Velde and E. J. Baerends, *Theor. Chem. Acc.*, 1998, **99**, 391.

53 J. P. Perdew, *Phys. Rev. B*, 1986, **33**, 8822–8824.

54 A. Becke, *Phys. Rev. A*, 1988, **38**, 3098–3100.

55 E. van Lenthe and E. J. Baerends, *J. Comput. Chem.*, 2003, **24**, 1142.

56 B. Roos and P. R. Taylor, *Chem. Phys.*, 1980, **48**, 157–173.

57 H.-J. Werner and P. J. Knowles, *J. Chem. Phys.*, 1985, **82**, 5053–5063.

58 P. J. Knowles and H.-J. Werner, *Chem. Phys. Lett.*, 1985, **115**, 259–267.

59 H.-J. Werner, P. J. Knowles, R. Lindh, F. R. Manby, M. Schütz, P. Celani, T. Korona, A. Mitrushenkov, G. Rauhut, T. B. Adler and *et al.*, *MOLPRO, Version 2010.1, a Package of* Ab initio *Programs, Cardiff University: Cardiff, United Kingdom, and University of Stuttgart: Stuttgart, Germany*.

60 T. H. Dunning, *J. Chem. Phys.*, 1989, **90**, 1007.

61 D. E. Woon and T. H. Dunning, *J. Chem. Phys*, 1993, **98**,

1358–1372.

62 O. Legeza, QC-DMRG-Budapest, *A Program for Quantum Chemical DMRG Calculations.* Copyright 2000–2013, HAS RISSPO Budapest.

63 O. Legeza and J. Sólyom, *Phys. Rev. B*, 2003, **68**, 195116.

64 O. Legeza and J. Sólyom, *Phys. Rev. B*, 2004, **70**, 205118.

65 O. Legeza, J. Röder and B. A. Hess, *Phys. Rev. B*, 2003, **67**, 125114.

66 S. L. Altmann and P. Herzig, *Point-Group Theory Tables*, Oxford, 1994.

67 J. March, *Advanced Organic Chemistry: Reactions, Mechanisms, and Structure*, Wiley, 1992.

68 M. L. Abrams and C. D. Sherrill, *J. Chem. Phys.*, 2004, **121**, 9211.

69 S. Shaik, D. Danovich, W. Wu, P. Su, H. S. Rzepa and P. C. Hiberty, *Nature Chemistry*, 2012, **4**, 195–200.

70 D. Danovich, S. Shaik, H. S. Rzepa and R. Hoffmann, *Angew. Chem. Int. Ed.*, 2013, **52**, 5926–5928.

71 G. Frenking and M. Hermann, *Angew. Chem. Int. Ed.*, 2013, **52**, 2–6.

72 J. M. Matxain, F. Ruipérez, I. Infante, X. Lopez, J. M. Ugalde, G. Merino and M. Piris, *J. Chem. Phys.*, 2013, **138**, 151102.

73 L. T. Xu and T. H. Dunning, *J. Chem. Theory Comput.*, 2014, **10**, 195–201.

74 C. W. Bauschlicher and S. R. Langhoff, *J. Chem. Phys.*, 1987, **87**, 2919.

75 M. L. Abrams and C. D. Sherrill, *J. Chem. Phys.*, 2004, **121**, 9211.

76 C. D. Sherrill and P. Piecuch, *J. Chem. Phys.*, 2005, **122**, 124104.

77 F. A. Evangelista, *J. Chem. Phys.*, 2011, **134**, 224102.

78 J. S. Deheng Shi, Xiaoniu Zhang and Z. Zhu, *Mol. Phys.*, 2011, **109**, 1453–1465.

79 S. Wouters, W. Poelmans, P. W. Ayers and D. V. Neck, *arXiv:1312.2415*, 2013.

80 L. B. Roskop, L. Kong, E. F. Valeev, M. S. Gordon and T. L. Windus, *J. Chem. Theory Comput.*, 2014, **10**, 90–101.

81 J. S. Boschen, D. Theis, K. Ruedenberg and T. L. Windus, *Theor. Chem. Acc.*, 2014, **133**, 1425.

82 L. Andrews and X. Wang, *J. Phys. Chem. A*, 2002, **106**, 7696–7702.

83 G. Trinquier and J.-P. Malrieu, *J. Am. Chem. Soc.*, 1987, **109**, 5303–5315.

84 J.-P. Malrieu and G. Trinquier, *J. Am. Chem. Soc.*, 1989, **111**, 5916–5921.

85 G. Trinquier, *J. Am. Chem. Soc.*, 1990, **112**, 2130–2131.

86 M. Bogey, H. Bolvin, C. Demuynck and J. L. Destombes, *Phys. Rev. Lett.*, 1991, **66**, 413–416.

87 M. Lein, A. Krapp and G. Frenking, *J. Am. Chem. Soc.*, 2005, **127**, 6290–6299.

88 D. B. Chesnut, *Heteroatom. Chem.*, 2002, **13**, 53–64.

89 A. J. Adamczyk and L. J. Broadbelt, *J. Phys. Chem. A*, 2011, **115**, 2409–2422.

90 L. C. Snyder and Z. R. Wasserman, *J. Comput. Chem.*, 1979, **6**, 5222–5225.

91 R. A. Poirier and J. D. Goddard, *Chem. Phys. Lett.*, 1981, **80**, 37–41.

92 H. Lischka and H.-J. Köhler, *Chem. Phys. Lett.*, 1982, **85**, 467–471.

93 A. F. Sax, *J. Comput. Chem.*, 1985, **6**, 469–477.

94 K. Krogh-Jespersen, *J. Am. Chem. Soc.*, 1985, **107**, 537–543.

95 G. Frenking and R. Tonner, *Science*, 2007, **318**, 746.

96 T. E. Gier, *J. Am. Chem. Soc.*, 1961, **83**, 1769–1770.

97 M. F. Lucas, M. C. Michelini, N. Russo and E. Sicilia, *J. Chem. Theory. Comput.*, 2008, **4**, 397–403.
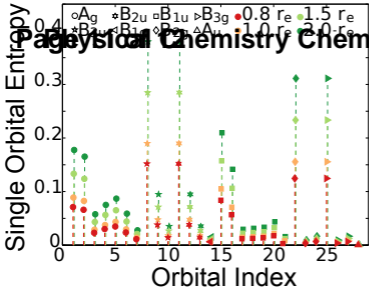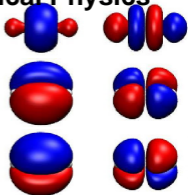
Graphical Abstract:

We present a quantum entanglement analysis to dissect the bond orders in polyatomic molecules.